Performance improvement of PVDF hollow fiber-based membrane distillation process

Yang, Xing; Wang, Rong; Shi, Lei; Fane, Anthony Gordon; Debowski, Marcin

2010

Yang, X., Wang, R., Shi, L., Fane, A. G., & Debowski, M. (2011). Performance improvement of PVDF hollow fiber-based membrane distillation process. Journal of Membrane Science, 369(1-2), 437-447.

https://hdl.handle.net/10356/98144

https://doi.org/10.1016/j.memsci.2010.12.020

Performance improvement of PVDF hollow fiber-based membrane distillation process

Xing Yang[1,2], Rong Wang*[,1,2], Lei Shi[1], Anthony G. Fane[1,2], Marcin Debowski[3]

1. Singapore Membrane Technology Centre, Nanyang Technological University, Singapore 639798
2. School of Civil and Environmental Engineering, Nanyang Technological University, Singapore 639798
3. Singapore Institute of Manufacturing Technology, Singapore 638075

*Corresponding author at: School of Civil and Environmental Engineering, Nanyang Technological University, 639798 Singapore, Singapore. Tel.: +65 6790 5327; fax: +65 6791 0676.

E-mail address: rwang@ntu.edu.sg (R. Wang).

Abstract

The performance of membrane distillation depends on both membrane and module characteristics. This paper describes strategies to improve the performance of hollow fiber membrane modules used in Direct Contact Membrane Distillation (DCMD).

Three different types of hydrophobic polyvinylidene fluoride (PVDF) hollow fiber membrane (unmodified, plasma modified and chemically modified) were used in this study of Direct Contact Membrane Distillation (DCMD). Compared to the unmodified PVDF hollow fiber membrane, both modified membranes showed greater hydrophobicity and mechanical strength, smaller maximum pore sizes and narrower pore size distributions, leading to more sustainable fluxes and higher water quality (distillate conductiviy < 1μs·cm^{-1}) over a one month test using synthetic seawater (3.5 wt% sodium chloride solutions). Comparing the plasma and chemical modification the latter has marginally better performance and provides potentially more homogeneous modification.

MD modules based on shell and tube configuration were tested to identify the effects of shell and lumen side flow rates, fiber length and packing density. The MD flux increased to an asymptotic value when shell-side Re_f was larger than 2500, while the permeate/lumen side reached an asymptotic value at much lower Re_p (>300). By comparing the performance of small and larger modules, it was found that it is important to utilize a higher shell-side *Re* in the operation to maintain a better mixing near the membrane surface in a larger module. Single fiber tests in combination with heat transfer analysis, verified that a critical

fiber length existed that is the required length to assure sufficient driving force along the fiber to maintain adequate MD performance. In addition, for multi-fiber modules the overall MD coefficient decreased with increasing packing density, possibly due to flow maldistribution. This study shows that more hydrophobic membranes with a small maximum pore size and higher liquid entry pressure are attainable and favorable for MD applications. In order to enhance MD performance various factors need to be considered to optimize fluid dynamics and module configurations, such as fiber length, packing density and the effect of module diameter and flow rates.

Keywords: PVDF hollow fiber membrane, modification, MD long-term performance, fluid dynamics, heat transfer, module characteristics.

1. **Introduction**

Membrane distillation (MD) is a thermally driven membrane separation process, which involves the transport of water vapor through micro-porous hydrophobic membranes from aqueous solutions. The driving force for vapor transport is the vapor pressure difference across the membrane caused by the temperature gradient between the hot-feed and cold-permeate. Among various MD processes, direct contact membrane distillation (DCMD) is the simplest mode because no external condenser is required, compared to vacuum membrane distillation (VMD) and sweep gas membrane distillation (SGMD) [1-4].

MD can yield highly purified distillate and deal with concentrated salt solutions/brines under mild operating conditions [1, 5], thus it has great potential to be applied in many applications, such as in desalination of seawater and brackish water and brine concentration. However, MD has some potential disadvantages, such as flux lowering due to poor hydrodynamics and inefficient module design [1] and distillate contamination due to membrane pore wetting [6, 7], the latter is one of the main factors hindering the wider application of MD technology.

The maintenance of the vapor phase in dry membrane pores during MD is an essential condition for process function. To avoid pore wetting, the membrane material has to be hydrophobic with a contact angle as high as possible and the membrane should have a relatively small maximum pore size. The hydrophobic micro-porous membranes such as those made from polytetrafluoroethylene (PTFE), polyvinylidene fluoride (PVDF),

polyethylene (PE) or polypropylene (PP) can fulfill the basic requirement of hydrophobicity. However, since most of these membranes are fabricated for other processes such as microfiltration (MF), they suffered drawbacks such the presence of some large pore sizes when applied to MD processes. The pore sizes are 'nominal' mean sizes and there will be a distribution including larger pores. The presence of larger pores is a possible reason causing membrane wetting even though the membranes are highly hydrophobic [8]. To improve the applicability of these membranes for the MD processes, there are two approaches to minimize wetting; one is a finely porous hydrophobic coating which helps to minimize the pores size while maintaining suitable porosity [9-11]; the other is to apply a dense hydrophilic coating which can protect the effective membrane pores from wetting [12-17]. The majority of modifications have been to apply a nonporous hydrophilic layer, but this is likely to add more resistance than a porous hydrophobic coating. Our approach is to evaluate hydrophobic coatings.

Most of the reported MD studies have focused on flat sheet membranes due to their availability in hydrophobic materials. This is particularly so for PTFE which is processed in sheet form. However, in industrial applications, which require a large membrane surface area per unit volume without supporting structure, hollow fiber-based membrane modules are considered more favorably. Additionally, as a thermally driven process, MD can be significantly affected by the temperature polarization if the hydrodynamic conditions deteriorate [18-20]. It has been shown that the hollow fiber module could potentially have the least temperature polarization among various module configurations [21].

However, there are limited reports available on improving fluid dynamics and designing hollow fiber modules for MD applications in the open literature [22-25]. Some relevant studies have focused on the effect of packing density, flow maldistribution and hydrodynamic behavior in the shell side of hollow fiber modules, based on studies of various gas-liquid/ liquid-liquid contactors [26-31]. It is widely accepted that non-ideal flow distribution leads to less active membrane area and insufficient mass transfer, and thus poor module performance. Generally, in order to increase membrane area and reduce module fabrication costs, larger module housings, higher packing density and/or longer fiber length are preferred in industry [32]. However, it has been observed in MD studies that the thermal efficiency can be impacted negatively by increasing packing density and fiber length because the distillate tends to be heated up along the fibers [10, 33]. In addition, the risk of membrane pore wetting increases with the increasing fiber length due to the imposed hydrostatic pressure drop along the module length [22].

In this study, we examine strategies to improve DCMD performance from two aspects: (1) modification of membrane surface properties; and (2) evaluation of certain hollow fiber module characteristics. Specifically, we have enhanced membrane hydophobicity, reduced membrane pore sizes by two types of modification treatment, and then compared the modified and unmodified membranes in terms of sustainable flux and long-term performance. In addition, the effects of fluid dynamics, fiber length, packing density and module diameter on the MD performance have been investigated based on heat transfer analysis. It is expected that this study can help identify potential approaches to overcome

the commonly encountered problem of membrane wetting and mitigate the concentration/temperature polarization effects to facilitate practical applications of the MD process.

2. Experimental

2.1 Membrane material and modification methods

The unmodified membrane used in this study was a newly developed polyvinylidene fluoride (PVDF) hollow fiber membrane. To improve the membrane properties for better MD application, two surface modification methods were applied to modify the original PVDF hollow fiber membrane, as elaborated below.

2.1.1 Plasma modification

Plasma modification of the original PVDF hollow fiber membrane was conducted using a P2i plasma Enhancement Machine (model Ion Mask 40i) under a vacuum pressure of ~20 mmHg. The plasma coating involved a two-step process: 1) surface activation by exposing for the membrane a few seconds to a continuous plasma wave with some bleed of atmospheric gases where free radicals were introduced to the membrane surface; and 2) polymerization by bringing the membrane in contact with the vapor of activated monomer for a period of time. During this step the plasma was induced in a pulse manner limiting destructive fragmentation of the monomer. The monomer specifically used to produce the

hydrophobic polymeric nano-coating was 1H, 1H, 2H, 2H-perfluorodecyl acrylate. The process, as diffusion controlled, allowed the activated monomer to penetrate into the membrane pores. The degree of surface activation, the depth of deposition of the fluorinated polymer into the membrane, and the thickness of the grafted layer at the membrane surface can be adjusted by the plasma generation power and the operation time of the activation and polymerization steps respectively. To get an optimal membrane performance in this study, the polymer deposition time was adjusted from 14 to 21 milliseconds, while the activation time and the plasma power at the activation and polymerization stages were kept constant throughout the process. For the comparative performance tests amongst various membranes in the present work, plasma-treated fibers with deposition time 21 ms were used.

2.1.2 Chemical modification

The chemical modification involved the hydroxylation of the PVDF membrane by an aqueous lithium hydroxide (LiOH) solution and successive reduction with an organic sodium borohydride ($NaBH_4$) solution followed by cross-linking with a perfluoro-compound of perfluoropolyether containing ethoxysilane terminal groups.

Firstly, the PVDF hollow fiber membranes were immersed into a LiOH aqueous solution (1 to 2M) under magnetic stirring for 12 hours, then rinsed with deionized (DI) water for three times and subsequently with IPA once. After rinsing, the membranes were dried under room temperature. The LiOH-treated PVDF membranes were then immersed in a $NaBH_4$ organic solution under magnetic stirring for 12 hours. After the $NaBH_4$ treatment,

the membranes were rinsed with the following liquids of IPA, 1:1 v/v HCl/Ethanol mixture and 1:1 v/v Acetone aqueous solution in sequence. To complete this reduction step and impart the hydroxyl function group (-OH) to the membrane, the hollow fibers were dried under vacuum at 40°C. After these pretreatment steps, the chemical crosslinking using a perfluoropolyether with ethoxysilane terminal groups, which are apt to chemically bond the -OH sites, was performed in the oven for 30mins at 100°C.

2.2 Membrane characterization

2.2.1 Measurements of hollow fiber membrane's liquid entry pressure of water (LEPw), porosity and pore size distribution

The measurement of LEPw was conducted using dead-end hollow fiber modules containing 3−5 fibers. The detailed methodology can be found elsewhere [34]. It should be noted that the pressure at which a continuous flow of water was observed on the permeate side was assumed to be the membrane LEPw, as defined in literature [34]. The Laplace equation provides the relationship between the maximum pore size, LEPw and the related operating conditions [1]:

$$LEPw > \Delta P_{interface} = P_{liquid} - P_{vapor} = \frac{-2B\gamma_L \cos\theta}{r_{max}} \qquad (1)$$

where B is a geometric factor determined by pore structure, γ_L is the liquid surface tension and θ is the liquid/solid contact angle. The membrane pores will be subject to wetting once the operating pressure exceeds the LEPw.

The membrane porosity is defined as the volume of the pores divided by the total

volume of the membrane. It can be determined by comparing the density of the polymer material using isopropyl alcohol (IPA, analytical grade from VWR Co Ltd), which penetrates into the pores of the membrane, and the density of the membrane using pure water, which does not enter the pores. The detailed methodology was proposed by Smolders and Franken [34].

The pore size distribution were determined by a capillary flow porometer (model CFP 1500A, from Porous Material. Inc (PMI)), whose working principle is based on the bubble-point and gas permeation tests [35]. The hollow fiber samples were potted into the sample holder and soaked by the wetting fluid (Galwick, with surface tension 15.9 x 10^{-3} N/m) till completely wet. During the test, the gas flow rate was increased stepwise and passed through the saturated sample until the applied pressure exceeded the capillary attraction of the fluid in the pores. By comparing the gas flow rates of a wet and dry sample at the same pressures, the percentage of flow passing through the pores larger than or equal to the specified size can be calculated from the pressure-size relationship.

2.2.2 Measurements of dynamic contact angle, mechanical strength and membrane morphology

Dynamic contact angle was measured by a tensiometer (DCAT11 Dataphysics, Germany). A sample fiber glued to the holder was hung from the arm of an electro-balance, and then put through a cycle of immersions into deionized (DI) water. The contact angle

was calculated from the wetting force based on the Wihelmy method.

The mechanical strength of the fibers was measured using a Zwick 0.5kN Universal Testing Machine at room temperature. The sample was clamped at both ends and pulled under tension at a constant elongation velocity of 50 mm·min^{-1}. Tensile modulus and tensile stress at the break point were measured to indicate the mechanical strength of the fibers and the degree of deformation under a given load.

To observe the morphologies of the original and modified PVDF hollow fiber membranes, dried membrane samples were fractured in liquid nitrogen and sputtered with a thin layer of gold. The cross-section and inner/outer surface of the hollow fiber membranes were examined using a Zeiss EVO 50 Scanning Electron Microscope (SEM).

2.3 Membrane module fabrication

Lab-scale MD modules were fabricated by potting the unmodified and modified PVDF hollow fiber membranes into Teflon housings. The specifications of all modules are listed in Table 1. Two different sizes of teflon housing (9.5 mm and 19 mm) were used in the current study. Regular modules, type #1 (9.5 mm housing) were packed with various types of membrane and were used for flux assessment. Modules #1 (9.5 mm housing) and #2 (19 mm housing) packed with unmodified fibers were compared in the investigation of module diameter**.** Single-fiber modules (#3), which contained only one straight fiber with

various lengths ranging from 150 mm to 1020 mm were made to investigate the effect of fiber length. Module #4 (19 mm housing) of different lengths (450 mm and 650 mm, respectively) and different packing densities (3.5% – 71%) were used in the packing density study.

2.4 MD performance tests

The MD experimental setup is shown in Fig. 1. Both the feed and permeate solutions were cycled through the hollow fiber module in countercurrent mode. On the shell side, the feed solution (synthetic seawater: 3.5 wt% sodium chloride (NaCl) with conductivity around 60 ms·cm^{-1}), was heated (in the range 313K – 343K) and circulated by a peristaltic pump (0 – 12 L·min^{-1}). On the lumen side, the permeate (pure water, with conductivity around 0.5 μs·cm^{-1}) was cooled down to 298K by a cooling circulator and cycled by another peristaltic pump (0 – 4 L·min^{-1}). The distillate was collected in an overflow tank sitting on a balance (±0.1 g).

3. Theory of mass/heat transfer in MD

In all membrane separation processes, the permeation flux N can be calculated from experimental results by applying the following equation:

$$N = \frac{m}{A * \Delta t} \tag{2}$$

where m is the mass of the permeate, kg, A the effective membrane area, m^2, and Δt the

time interval, *h*. The transmembrane flux can be also calculated by the product of a transfer coefficient and the driving force, and in MD it can be expressed as:

$$N = C * \Delta P = C * (P_1 - P_2) \quad (3)$$

where C is the membrane distillation coefficient, $kg \cdot m^{-2} \cdot h^{-1} \cdot kPa^{-1}$. $\Delta P = (P_1 - P_2)$ is the driving force, which, for an average 'module value', is the logarithmic mean vapor pressure difference of the feed and permeate, kPa. If C is based on bulk temperature/vapour pressure values it is an 'overall' coefficient that includes the intrinsic membrane coefficient, C_i and boundary layer effects. According to the mass transfer models [3], C_i is dependent on the membrane pore geometries and the operating temperature.

According to previous studies [36], the effect of the concentration polarization on the vapour pressure driving force can be ignored due to the relatively weak effect of salt concentration on vapour pressure. Thus the vapor flux through the membrane is mainly driven by the vapor pressure difference resulting from the temperature difference. The total heat transport in MD consists of conductive heat through the membrane and the latent heat contributing to the vapor flux [21]:

$$Q = Q_c + Q_v = (k_m / \delta_m)(T_{fm} - T_{pm}) + NH_{V,T} \quad (4)$$

where $H_{V,T}$ is the latent heat of evaporation ($kJ \cdot kg^{-1}$), which can be determined from enthalpy data [37, 38]; T_{fm} and T_{pm} are the temperatures at the membrane walls adjacent to the feed and permeate, respectively, δ_m is the wall thickness of the membrane, and k_m is the overall thermal conductivity of the porous membrane. The value for k_m of the original PVDF fiber used in this study is taken as 319.6 $W \cdot m^{-1} \cdot K^{-1}$ based on the method provided

by Sarti et al [39].

Since temperature polarization commonly exists in MD processes [21], the wall temperatures may be significantly different from the bulk temperatures. In order to estimate the actual driving force across the membrane and investigate the temperature polarization effect, the wall temperatures T_{fm} and T_{pm} can be determined from heat transfer relationships [40]:

$$T_{fm} = T_f - (T_f - T_p)\frac{1/h_f * d_i/d_o}{1/h_f * d_i/d_o + 1/(h_m + h_v) + 1/h_p} \tag{5}$$

$$T_{pm} = T_p + (T_f - T_p)\frac{1/h_p}{1/h_f * d_i/d_o + 1/(h_m + h_v) + 1/h_p} \tag{6}$$

where $h_m = \frac{k_m}{\delta_m}$ ($\mathrm{W \cdot m^{-2} \cdot K^{-1}}$), h_v is the heat transfer coefficient associated with vapour flow and h_f and h_p are the liquid film heat transfer coefficients on the feed and permeate sides, respectively. By assuming Q_v is constant at the average membrane temperature T_m, the vapor heat transfer coefficient h_v is given by [3]:

$$h_v = \frac{NH_{V,Tm}}{\Delta T_m} = \frac{NH_{V,\frac{T_{fm}+T_{pm}}{2}}}{(T_{fm} - T_{pm})} \tag{7}$$

Thus, the overall heat transfer coefficient can be expressed as:

$$U = \left(\frac{1}{h_f} * \frac{d_i}{d_o} + \frac{1}{h_m + h_v} + \frac{1}{h_p} \right)^{-1} \tag{8}$$

Here $R_{OV} = \frac{1}{U}$ is the overall transfer resistance, and $R_f = \frac{1}{h_f} * \frac{d_i}{d_o}$, $R_p = \frac{1}{h_p}$ and $R_m = \frac{1}{h_m + h_v}$ are the individual resistances for the feed film, permeate film and the membrane, respectively. The film heat transfer coefficients h_f and h_p can be expressed in terms of the

Nusselt number ($Nu_i = \frac{h_i d_h}{k_i}$), which is correlated with Reynolds number ($Re = \frac{d_h v \rho}{\mu}$) and Prandtl number ($Pr = \frac{c_p \mu}{k}$) through the Graetz-Lévêque equation under laminar conditions [21, 41]:

$$Nu = 1.86 (RePr \frac{d_h}{L})^{0.33} \quad (9)$$

where L is the fiber length and d_h is the hydraulic diameter of the flow channel. Based on Eq (9), h_f and h_p can be estimated under given operating conditions, thus the local film resistance R_i can be obtained correspondingly. It should be noted that all heat fluxes mentioned in the above equations were based on the inner surface of the hollow fibers.

4. Results and discussion

4.1 Membrane Characterization

The SEM pictures, which show the morphologies of the outer and inner surfaces and the cross-section of the unmodified and modified PVDF membranes, are presented in Fig. 2. It was observed that the outer surface of the unmodified PVDF membrane was relatively smooth, while the surface became rougher after grafting with the fluoro-compounds, and the roughness tended to increase significantly after chemical modification (Fig. 2a). As for the inner surface morphology (Fig. 2b), both the pore size and the number of pores have been reduced visibly after the modifications. This is not surprising for the membrane treated by the chemical method, as the whole membrane was immersed into the chemical solution and the modification occurred throughout the entire membrane. For the plasma treated membrane, the results suggest that the activated poly-fluoro monomer has

penetrated into the membrane pores during the plasma treatment. By observing the cross-section morphology (Fig. 2c), it can be seen that the sponge-like structure became tighter after the modifications.

Table 2 shows the basic characteristics of the three types of membranes, which include the fiber dimensions, contact angle, porosity, LEPw and mechanical strength. It can be seen that the unmodified PVDF membrane has a very high porosity but relatively poor hydrophobic properties and low LEPw. After the plasma modification, the contact angle and LEPw increased by 20% and 180%, respectively. The chemical modification also improved the contact angle and LEPw of the original PVDF membrane by 30% and 164%, respectively. In addition, both of the modification methods helped to improve the mechanical strength of the fibers.

The membrane pore size and pore size distributions (number %) are illustrated in Fig. 3. The unmodified PVDF membrane had a distinct bimodal distribution (Fig. 3a). Compared to the unmodified membrane which has a maximum pore size of 0.421 μm and mean pore size of 0.064 μm, both modified membranes have much narrower pore size distributions and smaller maximum pore sizes (0.191 μm and 0.189 μm for the plasma and chemical methods respectively). This is due to the introduction of poly-fluoro monomers to the membrane surfaces that have restricted some of the big pores and blocked off some of the small pores in the plasma treatment. In the chemical modification process, the hydroxyl functionized PVDF molecules were cross-linked through fluoro-compound

macromolecules, which formed a network on the membrane surface and also the bulk membrane, leading to a reduction of the effective membrane pore size. Fig. 3c shows that the chemically modified membrane had the narrowest size distribution. These results are consistent with the change in the LEPw values. The smaller pore sizes of the modified membranes lead to much higher LEPw, as indicated in Table 2. As a result, it is anticipated that the modified membranes would be less vulnerable to membrane pore-wetting but have correspondingly lower fluxes.

4.2 MD flux assessment of unmodified and modified membranes

Fig. 4 shows the permeation flux as a function of feed water temperature for the three membranes under the same operating conditions. The fluxes of the unmodified PVDF, plasma and chemically modified membranes all exhibited an exponential dependence on temperature, as anticipated by the vapor pressure of water versus temperature relationship given by the Antoine equation [42]:

$$P = \exp(23.20 - \frac{3816.44}{T - 46.13}) \quad (13)$$

It can be seen that the modified membranes presented similar fluxes to the unmodified one at low operating temperatures, but about 20% flux reduction was found at the operating temperature of 70°C. The reasons for the flux reduction were the partial closure of pores, loss of large pores and overall decrease in the porosity after the modifications. In order to assess flux stability the three types of membrane were compared in long-term tests.

Fig. 5 illustrates the flux and permeate conductivity of the three membranes over a long period of operation (200 to >600 hours). It can be seen that all of the membranes delivered sustainable fluxes for an extended period but, for the unmodified PVDF membrane, there was a slow and gradual conductivity build-up of the distillate followed by a sudden increase after about one-week (ca 170 hours). This indicates that this membrane was subject to pore wetting and further deterioration of the water quality was expected. In contrast the distillate conductivity obtained from the plasma modified membrane remained below 1.0 $\mu s \cdot cm^{-1}$, and the chemically modified membrane resulted in more stable performance and even better water quality (<0.5 $\mu s \cdot cm^{-1}$) over one-month of testing. Therefore, the advantage of the modified hollow fiber membranes over the unmodified is the greatly reduced of membrane pore wetting, ensuring effectively 100% salt rejection. The chemically modified membrane achieved this non-wetting performance at a modest flux penalty (<20% lower).

4.3 Effects of fluid dynamics

One of the approaches to enhance the mass and heat transfer inside the hollow fiber modules is to improve the hydrodynamic conditions adjacent to the membrane surface, i.e. to optimize the flow velocity of the feed in the shell side. Fig. 6 shows the effect of the feed circulation velocity in terms of Reynolds number (Re_f) on the permeation flux. For the smaller module (9.5-mm housing) the MD flux remained unchanged when the flow rate was varied from 2 to 7.5 $L \cdot m^{-3}$ (corresponding to Re_f: 2500 to 9420). This may be due to

the fact that the feed stream had reached turbulence (Re_f>2500) within this range and the shell-side was no longer the controlling transport resistance. For the bigger module #2 (19-mm housing), the permeation flux initially increased with increasing circulating velocity and then tended to an asymptotic value when entering the turbulent region (Re_f >2500) signifying a shift to lumen-side controlling resistance, However, the maximum flux obtained in the big module was lower than the small module under the same operating conditions. The difference was probably caused by the lower (lumen-side) Re_p in the larger module due to the similar permeate flow rates used in both modules. The greater fiber length in the larger module would have also contributed to the difference (see section 4.4).

It has been widely reported that a higher feed circulation velocity (i.e. higher mixing intensity) can help to reduce the thickness of the boundary layer adjacent to membrane surface [6, 43, 44], which is favorable for the mitigation of concentration and temperature polarization, and to maximize the driving force between the feed and permeate sides. However higher pumping energy is required to provide a higher feed circulation velocity. From this study, it was found that a moderate feed circulation velocity can be chosen based on the demand of satisfactory permeation flux and there is no added benefit in increasing flow rate once turbulence is reached.

On the other hand, the lumen-side permeate circulation velocity is also an important factor to be considered. Increase in the permeate circulation velocity can improve the heat transfer on the permeate side by reducing the temperature polarization effect (the effect of

concentration polarization is negligible since the permeate fluid in this DCMD study is distilled water). By minimizing the thermal boundary layer on the permeate side, the temperature at the membrane surface approaches the temperature in the bulk permeate and consequently the driving force can be maximized. However, the greater effect would be the rise in the bulk temperature of the permeate at lower lumen flow. This affects the driving force at the permeate outlet region.

Fig. 7 shows the effect of permeate circulation velocity in terms of Re_p on the permeation flux. Since the permeate flowed through the lumen of the hollow fiber, a much low velocity in the lumen was used. It can be seen that the permeation flux firstly increased significantly at low *Re* range (Re_p<300), and then reached a steady asymptotic value when Re_p was higher than 300. The possible reason causing this early onset of the steady-state may be the increased transverse vapor flux that helped break down the laminar boundary layer, thus greatly enhancing the mixing on the membrane surface and facilitating the heat transfer at the permeate side. Consequently, the local film heat transfer (h_p) may not act as a controlling step even when the flow was still under laminar condition. Therefore, based on this study, a reasonably low circulation velocity can be chosen to optimize the MD performance with relatively low energy consumption.

4.4 Effects of membrane module configurations

4.4.1 Module size

Fig. 8 presents the MD fluxes of the small module and the big modules at different

feed temperatures. The flow rates of the feed and permeate for the two modules were kept the same, hence their Reynolds numbers were different. The results showed that the permeation flux increased exponentially with increasing feed temperature from both modules. In evaluating the performance of the larger module #2, several factors should be considered. Firstly, since the large module #2 was operated at a much lower *Re*, which would result in a thicker boundary layer and hence more severe temperature polarization, the mass/heat transfer would be less efficient. This situation would be worse at a higher temperature, as observed. Secondly, the greater length should be taken into account, as performance decreased with increasing fiber length (further discussion is provided in section 4.4.2). Thirdly, there would be greater tendency to flow maldistribution through the wider flow channel provided in the larger module. A comparison of the two modules can be made by correcting for the size effects in terms of *Re* and fiber length, based on the relationship between flux *N*, *Re* and *L* derived by fitting the experimental results. For example, the large module data in Fig. 6 can be correlated by,

$$N(big) = 2.86 + 5.15\left(\frac{Re}{Ld_h^{\,2}}\right)^{0.3} \quad (R^2=0.992) \tag{14}$$

Thus, in an ideal case with the same operating temperatures (T_f=323K, T_p =298K) and flow rates (Q_f =3 L·min^{-1}), for a small module of different *Re,* d_h and *L*, the predicted flux *N* would be 7.53 kg·m^{-2}·h^{-1} based on this equation. However, the actual flux of the small module reached 9.92 kg·m^{-2}·h^{-1} which was 30% higher than the predicted value. Having allowed for differences in *Re,* d_h and *L* the only significant difference between the small and large modules would be flow maldistribution which would worsen the transport processes in the larger module. To avoid these problems, improved mixing and appropriate fiber arrangement inside the housing are essential in scale-up to larger MD modules.

4.4.2 Fiber Length

To investigate the length effect of different modules, the relationships between MD coefficient, C, film transfer resistance R_i and fiber length, L, were plotted. In this case, C is the overall experimental MD coefficient from Eq. (3) with the log-mean vapour pressures based on bulk temperatures. It is clearly shown in Fig. 9a that the MD coefficient decreased dramatically with increasing fiber length in the beginning, and then gradually reached a steady state after a certain length (840 mm) in this current study. Though the feed side transfer resistances R_f played a dominant role in the mass transfer process over the range tested, all transfer resistances R_i increased with increasing fiber length and gradually reached asymptotic values at the same inflection point as the C curve. Hence, we defined a critical fiber length L_C which indicates the fiber length when the inflection point was reached. The corresponding temperature distributions on the membrane walls can be seen from Fig. 9b. With an increase in fiber length, T_{fm} eventually approached T_{pm} resulting in no contribution to the flux. The decrease in the driving force across the membrane with increasing fiber length can be viewed in Fig. 9c, which illustrates the development of thermal boundary layers by varying the fiber length. Initially the MD coefficient decreased and local resistance increased dramatically with increasing length due to the rapid build-up of thermal boundary layers which reduced the temperature difference across the membrane and inhibited the mass and heat transfer. Also more conduction heat loss would be expected at lower wall temperatures when L <840 mm [3]. However, with further increase in the fiber length (L >840 mm), the extremely low temperature gradient across the membrane at

the end of the fiber would have had negligible differential contribution to the flux. Hence, the critical fiber length L_C is effectively the operational fiber length that contributes to the major portion of the mass transfer of vapor through the membrane. It should be noted that the specific values of critical length may be different with varying module specifications and operating conditions. Although a longer module and thus a larger membrane area could result in higher water production, it is important to identify a critical fiber length to assure that the driving force along the fiber is sufficient to maintain a high efficiency. It is detrimental to make the module too long, as it involves compromise of capital and operating costs in industrial applications.

4.4.3 Fiber Packing Density

The MD coefficient as a function of the packing density is shown in Fig. 10, to further explore the hydrodynamic behavior and the flow mal-distribution in a ϕ randomly packed hollow fiber module. The experimental results obtained from the 450 mm-long module and the 650 mm-long module reveal that the overall MD coefficient decreased with increasing packing density. A very high MD coefficient was obtained in the extremely low packing density (<5%), probably due to the local turbulence caused by the presence of transverse flow in a loosely packed module where each fiber had full contact with the two fluids. A dramatic decrease in the overall MD coefficient was observed when the packing density increased in the lower packing density range (5% – 40%). This may be due to the uneven flow distribution of flow around each fiber and the channeling problems in the module. In

addition, it should be noted that these modules were tested under the same flow rate, thus both Re_f and Re_p decreased significantly with increasing packing density ϕ. Based on hydraulic calculations, the Re_f ranged from 4700 (ϕ=3.5%) to 1100 (ϕ=40%) and the Re_p decreased accordingly because of the increasing number of fibers. Therefore, the hydrodynamic conditions at the membrane surface deteriorated from loosely packed to tightly packed modules. This would also worsen the mass and heat transfer processes. However, when the packing density further increased up to an extremely high value (40% – 71%), the MD coefficient only decreased marginally. This may be due to relatively minor changes in the fluid dynamics in the shell side (Re_f decreased gradually from 1100 to 674). It should be noticed that a similarly complex relationship between the packing density and module performance were observed in many studies involving shell-side flow distribution when using gas-liquid hollow fiber membrane contactors [27, 28, 30, 32, 45].

5. Conclusions

In this work, two main strategies for MD process improvement have been executed. With respect to the membrane, three different types of hydrophobic hollow fiber membrane were evaluated for MD applications. It was found that a potential pore-wetting problem existed for the unmodified PVDF hollow fiber membrane due to its relatively low hydrophobicity and liquid entry pressure of water (LEPw). In contrast, both plasma and chemically modified PVDF hollow fiber membranes presented much higher contact angles, LEPw and mechanical strength, and smaller maximum pore sizes and narrower pore size

distributions. The modified membranes tended to be less vulnerable to the pore-wetting and able to maintain reasonably high MD flux in long-term operation. The chemically modified membrane had the narrowest pore size distribution and the best overall performance, in terms of stable flux and permeate quality.

Due to the complex combination of mass and heat transfer in this thermally driven process, the driving force and the MD coefficient are closely related to the fluid dynamics and MD module configuration. It was found that, the MD flux increased to an asymptotic value when Re_f was larger than 2500, while the stream on the permeate/lumen side reached asymptotic behaviour at much lower Re_p (>300). By comparing the performance of small and larger modules, it was shown that there are likely to be scale-up issues and that it is important to use a higher *Re* in the operation to maintain adequate mixing in a larger module. Single fiber tests in combination with heat transfer analysis, showed that a critical length existed that is the operational length to assure sufficient driving force along the fiber to maintain a high MD efficiency. In addition, the MD coefficient decreased with increasing packing density (randomly packed from 3.5% to 71%).

In summary, this study suggests that more hydrophobic membranes with small maximum pore size and higher LEPw are favorable for MD applications, and optimized fluid dynamics and module configurations (module size, length, packing density) should also be considered. Therefore, precautions must be taken during MD module scale-up.

Acknowledgments

The authors thank the Singapore Environment and Water Industry Council for funding the Singapore Membrane Technology Centre (SMTC) where this study was performed. Support from Siemens Water Technology is also gratefully acknowledged.

Nomenclature

A	Effective membrane area, m^2
B	Geometric factor determined by pore structure
C	Membrane distillation coefficient, $kg \cdot m^{-2} \cdot h^{-1} \cdot kPa^{-1}$
C_b	Bulk concentration of salt solution, $kg \cdot m^{-3}$ or wt %
C_m	Salt concentration at the membrane surface, $kg \cdot m^{-3}$ or wt %
c_p	Specific heat of the fluids, $J \cdot kg^{-1} \cdot K^{-1}$
d_h	Hydraulic diameter of the flowing channels, mm
d_i	Inner diameter of the hollow fiber, mm
d_o	Outer diameter of the hollow fiber, mm
d_s	Housing diameter of the module, mm
E_t	Tensile modulus, MPa
h_f	Film heat transfer coefficients from feed side, $W \cdot m^{-2} \cdot K^{-1}$
h_m	Heat transfer coefficient of the membrane, $W \cdot m^{-2} \cdot K^{-1}$
h_p	Film heat transfer coefficients from permeate side, $W \cdot m^{-2} \cdot K^{-1}$
h_v	Vapor heat transfer coefficient, $W \cdot m^{-2} \cdot K^{-1}$

$H_{V,T}$ Latent heat of evaporation, $kJ \cdot kg^{-1}$

k Thermal conductivity of liquids, $W \cdot m^{-1} \cdot K^{-1}$

L Effective fiber length, mm

L_C Critical fiber length, mm

m Mass of the permeate, kg

n Number of fibers

N Vapor flux, $kg \cdot m^{-2} \cdot h^{-1}$

Nu Nusselt number

P_1 Partial pressure of the vapor at the feed side, kPa

P_2 Partial pressure of the vapor at the permeate side, kPa

$\Delta P_{interface}$ Pressure drop on the membrane surface, kPa

P_{liquid} Hydrostatic pressure on the membrane surface of the feed side, kPa

Pr Prandtl number, $\frac{c_p \mu}{k}$

P_{vapor} Partial pressure in the membrane pores, kPa

Q Heat flux, $W \cdot m^{-2}$

Q_c Conductive heat flux through the membrane, $W \cdot m^{-2}$

Q_f Feed circulating flow rate, $L\ min^{-1}$

Q_p Permeate circulating flow rate, $L\ min^{-1}$

Q_v Latent heat of evaporation, $W \cdot m^{-2}$

r_{max} Maximum pore size , μm

Re Reynolds number, $\frac{d_h v \rho}{\mu}$

R_{OV} Overall transfer resistance, $m^2 \cdot K \cdot W^{-1}$

R_f Local transfer resistance of the feed side, $m^2 \cdot K \cdot W^{-1}$

R_m Local transfer resistance of membrane, $m^2 \cdot K \cdot W^{-1}$

R_p Local transfer resistance of the permeate side, $m^2 \cdot K \cdot W^{-1}$

T_f Bulk temperature of the feed , K

T_{fm} Temperature at the membrane surface on the feed side, K

T_m Average membrane temperature, K

T_p Bulk temperature of the permeate, K

T_{pm} Temperature at the membrane surface on the permeate side, K

U Overall heat transfer coefficient, $W \cdot m^{-2} \cdot K^{-1}$

v_f Circulating velocity of the feed, $m \cdot s^{-1}$

v_p Circulating velocity of the permeate, $m \cdot s^{-1}$

Greek letters

γ_L Surface tension, $N \cdot m^{-1}$

ε Membrane porosity, %

ϕ Module packing density, %

τ Membrane tortuosity

θ Liquid/solid contact angle

δ_b Strain at break, %

δ_m Membrane thickness, μm

δ_{tf} Thickness of the thermal boundary layer on the hot side, μm

δ_{tp} Thickness of the thermal boundary layer on the cold side, μm

δ_x Thickness of the concentration boundary layer, μm

μ Viscosity of the fluids, $Pa \cdot s^{-1}$

Suffix

f	Feed
i	Location, *i=f, p*
p	Permeate

References

[1] K. W. Lawson and D. R. Lloyd, Membrane distillation, Journal of Membrane Science, 124 (1) (1997) 1-25

[2] M. Khayet, P. Godino and J. I. Mengual, Theory and experiments on sweeping gas membrane distillation, Journal of Membrane Science, 165 (2000) 261-272

[3] J. Phattaranawik, R. Jiraratananon and A. G. Fane, Heat transport and membrane distillation coefficients in direct contact membrane distillation, Journal of Membrane Science 212 (2003) 177-193

[4] M. Khayet, M.P. Godino and J. I. Mengual, Thermal boundary layers in sweeping gas membrane distillation processes, AIChE Journal 48 (7) (2002) 1488-1497

[5] K. Karakulski, M. Gryta and A. Morawski, Membrane processes for portable water quality improvement, Desalination, 145 (2002) 315-319

[6] F. A. Banat and J. Simandl, Theoretical and experimental study in membrane distillation, Desalination, 95

(1994) 39-52

[7] K. W. Lawson and D. R. Lloyd, Membrane distillation. I. Module design and performance evaluation using vacuum membrane distillation, Journal of Membrane Science, 120 (1) (1996) 111-121

[8] J. Phattaranawik, R. Jiraratananon and A. G. Fane, Effect of pore size distribution and air flux on mass transport in direct contact membrane distillation, Journal of Membrane Science 215 (2003) 75-85

[9] B. Li and K. K. Sirkar, Novel membrane and device for vacuum membrane distillation-based desalination process, J. Membr. Sci. , 257 (1-2) (2005) 60-75

[10] L. Song, B. Li, K. K. Sirkar and J. L. Gilron, Direct contact membrane distillation-based desalination: novel membranes, devices, larger-scale studies, and a model, Industrial & Engineering Chemistry Research, 46 (2007) 2307-2323

[11] Z. Jin, D. L. Yang, S. H. Zhang and X. G. Jian, Hydrophobic modification of poly(phthalazinone ether sulfone ketone) hollow fiber membrane for vacuum membrane distillation, J. Membr. Sci. , 310 (1-2) (2008) 20-27

[12] A. Chanachai, K. Meksup and R. Jiraratananon, Coating of hydrophobic hollow fiber PVDF membrane with chitosan for protection against wetting and flavor loss in

osmotic distillation process, Separation and Purification Technology, 72 (2) (2010) 217-224

[13] S. Bonyadi and T. S. Chung, Flux enhancement in membrane distillation by fabrication of dual layer hydrophilic-hydrophobic hollow fiber membranes, Journal of Membrane Science, 306 (1-2) (2007) 134-146

[14] M. Khayet, J. I. Mengual and T. Matsuura, Porous hydrophobic/hydrophilic composite membranes: Application in desalination using direct contact membrane distillation, Journal of Membrane Science 252 (1-2) (2005) 101-113

[15] Y. Wu, Y. Kong, X. Lin, W. Liu and J. Xu, Surface-modified hydrophilic membranes in membrane distillation, Journal of Membrane Science, 72 (2) (1992) 189-196

[16] M. Qtaishat, D. Rana, M. Khayet and T. Matsuura, Preparation and characterization of novel hydrophobic/hydrophilic polyetherimide composite membranes for desalination by direct contact membrane distillation, Journal of Membrane Science, 327 (1-2) (2009) 264-273

[17] M. Qtaishat, M. Khayet and T. Matsuura, Guidelines for preparation of higher flux hydrophobic/hydrophilic composite membranes for membrane distillation, Journal of Membrane Science, 329 (1-2) (2009) 193-200

[18] R. Schneider, W. Hölz, R. Wollbeck and S. Ripperger, Membranes and modules for transmembrane distillation, Journal of Membrane Science, 39 (1) (1988) 25-42

[19] P. Hogan, A. Sudjito, A. G. Fane and G. Morrison, Desalination by solar heated membrane distillation, Desalination, (81) (1991) 81-90

[20] F. Lagana, G. Barbieri and E. Drioli, Direct contact membrane distillation: modelling and concentration experiments, Journal of Membrane Science, 166 (2000) 1-11

[21] R. W. Schofield, A. G. Fane and C. J. Fell, Heat and mass transfer in membrane distillation, Journal of Membrane Science, (33) (1987) 299-313

[22] M. S. El-Bourawi, Z. Ding, R. Ma and M. Khayet, A framework for better understanding membrane distillation separation process, Journal of Membrane Science, 285 (1-2) (2006) 4-29

[23] Z. Ding, L. Liu and R. Ma, Study on the effect of flow maldistribution on the performance of the hollow fiber modules used in membrane distillation, Journal of Membrane Science, 215 (2003) 11-23

[24] L.H. Cheng, P.C. Wu and J. Chen, Modeling and optimization of hollow fiber DCMD module for desalination, Journal of Membrane Science, 318 (2008) 154–166

[25] M. M. Teoh, S. Bonyadi and T.-S. Chung, Investigation of different hollow fiber module designs for flux enhancement in the membrane distillation process, Journal of Membrane Science, 311 (1-2) (2008) 371-379

[26] I. Noda, D. G. Brown-West and C. C. Gryte, Effect of flow maldistribution on hollow fibre dialysis-experimental studies, Journal of Membrane Science 5(1979) 209-225

[27] R. Prasad and K. K. Sirkar, Dispersion-free solvent extraction with microporous hollow-fiber modules, AIChE Journal 34 (2) (1988) 177

[28] M. J. Costello, A. G. Fane, P. A. Hogan and R. W. Schofield, The effect of shell side hydrodynamics on the performance of axial flowhollowfibre modules, Journal of Membrane Science, 80 (1993) 1-11

[29] J. Lemanski and G. G. Lipscomb, Effect of shell-side flows on hollow fiber membrane device performance, AIChE Journal 41 (1995) 2322-2326

[30] J. Wu and V. Chen, Shell-side mass transfer performance of randomly packed hollow fiber modules, Journal of Membrane Science 172 (2000) 59-74

[31] J. Zheng, Y. Xu and Z. K. Xu, Flow distribution in a randomly packed hollow fiber membrane module, Journal of Membrane Science 211 (2003) 263-269

[32] R. Thanedgunbaworn, R. Jiraratananon and M.H.Nguyen, Shell-side mass transfer of hollow fibre modules in osmotic distillation process, Journal of Membrane Science, 290 (2007) 105-113

[33] L. Cheng, P. Wu and J. Chen, Modeling and optimization of hollow fiber DCMD module for desalination, J. Membr. Sci., (318) (2008) 154–166

[34] C. A. Smolders and A. C. M. Franken, Terminology for membrane distillation, Desalination, 72 (1989) 249-262

[35] M. Khayet and T. Matsuura, Preparation and Characterization of Polyvinylidene Fluoride Membranes for Membrane Distillation, Industrial & Engineering Chemistry Research 40 (24) (2001) 5710-5718

[36] L. Martinez-Diez and M. I. Vazquez-Gonzalez, Temperature and concentration polarization in membrane distillation of aqueous salt solutions, Journal of Membrane Science 156 (1999) 265-273

[37] J. M. Smith and H. C. V. Ness, Introduction to Chemical Engineering Thermodynamics, 4th ed, McGraw-Hill, New York, 1990

[38] R. H. Perry, Perry's Chemical Engineers' Handbook, 6th ed, McGraw-Hill, New York, 1984

[39] G. C. Sarti, C. Gostoli and S. Matulli, Low energy cost desalination processes using hydrophobic membranes, Desalination, 56 (1985) 277-286

[40] V. A. Bui, L. T. T. Vu and M. H. Nguyen, Modelling the simultaneous heat and mass transfer of direct contact membrane distillation in hollow fibre modules, Journal of Membrane Science, 353 (2010) 85-93

[41] M. Tomaszewska, M. Gryta and A. W. Morawski, Study on the concentration of acids by membrane distillation, Journal of Membrane Science, 102 (1992) 113-122

[42] R. C. Reid, J. M. Prausnitz and T. K. Sherwood, The Properties of Gases and Liquids, 3rd edn., McGraw-Hill, New York, 1977

[43] S. Bouguccha, R. Chouilkh and M. Dhahbi, Numerical study of the coupled heat and mass transfer in membrane distillation, Desalination, 152 (2002) 245-252

[44] M. Khayet, M.P. Godino and J.I. Mengual, Possibility of nuclear desalination through various membrane distillation configurations: a comparative study: Khayet, M. et al. International Journal of Nuclear Desalination, Fuel and Energy Abstracts, 44 (6) (2003) 372-372

[45] F. Lipnizki and R. W. Field, Mass transfer performance for hollow fiber modules with shell-side axial feed flow: using an engineering approach to develop a framework, Journal of Membrane Science, 193 (2001) 195-208

List of Figures:

(3.5 % NaCl solution as feed Q_f =2.5 L·min^{-1}, Q_p =0.4 L·min^{-1}, T_p =298K, T_f =323K).

List of Tables

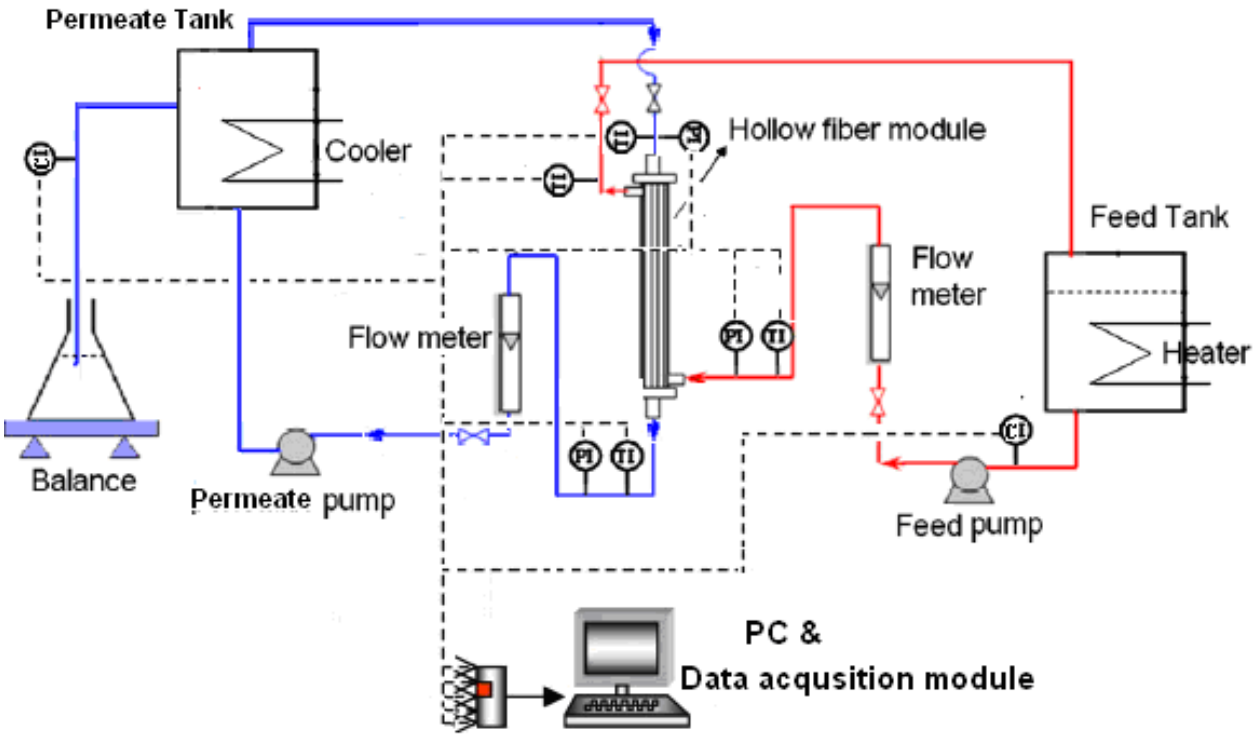
Permeate Tank
Cooler
Hollow fiber module
Feed Tank
Flow meter
Heater
Flow meter
Balance
Permeate pump
Feed pump
PC &
Data acqusition module

Fig. 1.

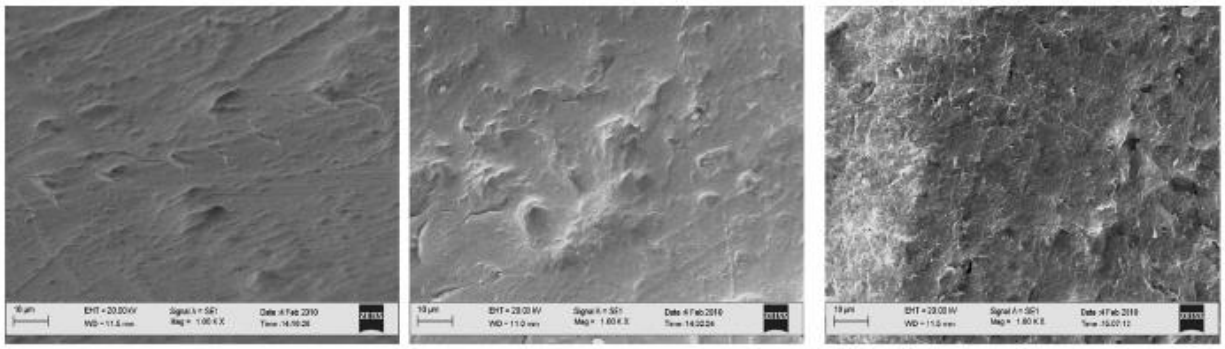

Original PVDF | Plasma modified | Chemically modified

a Outer surface 1000 x

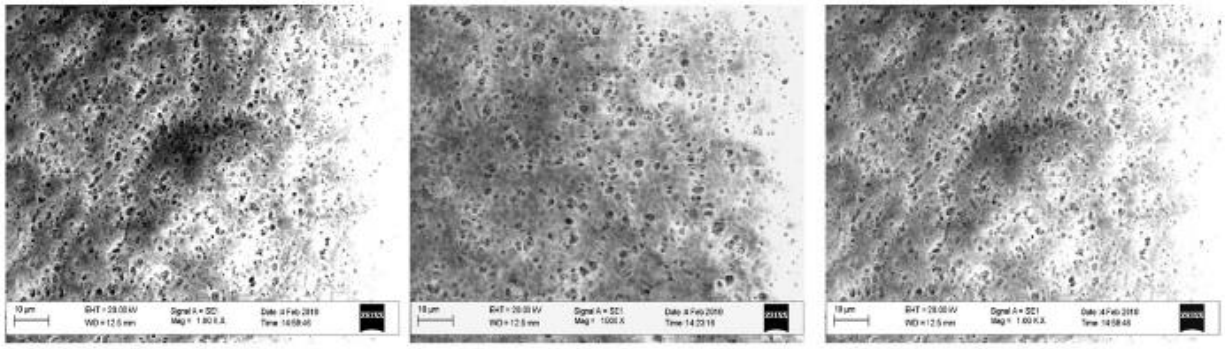

Original PVDF | Plasma modified | Chemically modified

b Inner surface 1000 x

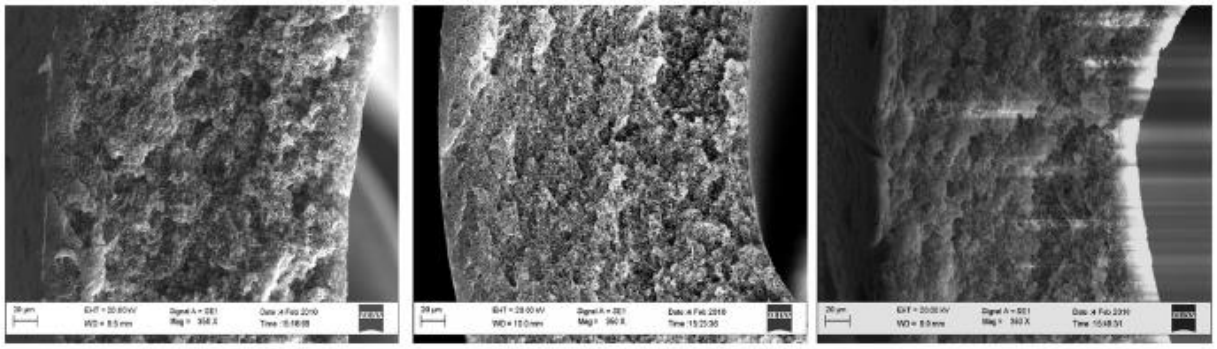

Original PVDF | Plasma modified | Chemically modified

c Cross-section 350 x

Fig. 2.

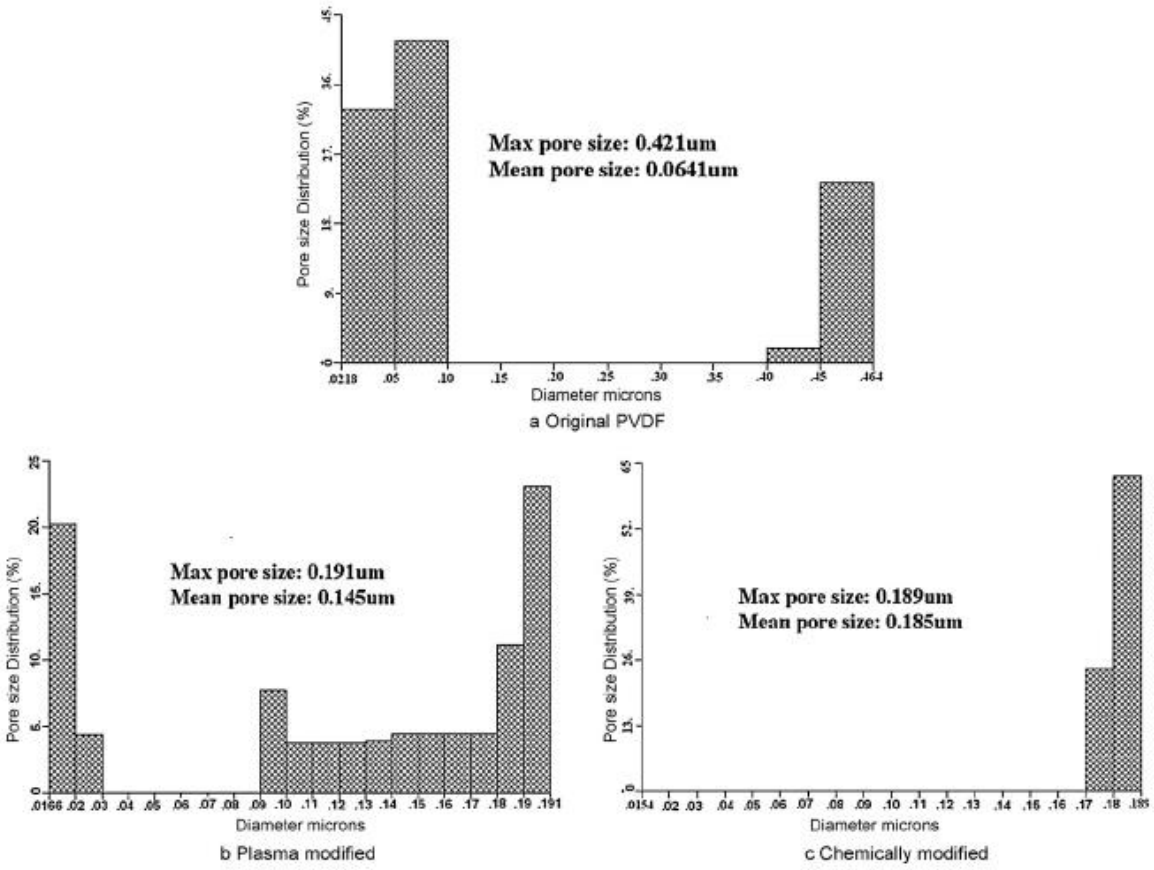
Pore size Distribution (%)
Max pore size: 0.421um
Mean pore size: 0.0641um
Diameter microns
a Original PVDF
Pore size Distribution (%)
Max pore size: 0.191um
Mean pore size: 0.145um
Diameter microns
b Plasma modified
Pore size Distribution (%)
Max pore size: 0.189um
Mean pore size: 0.185um
Diameter microns
c Chemically modified

Fig. 3.

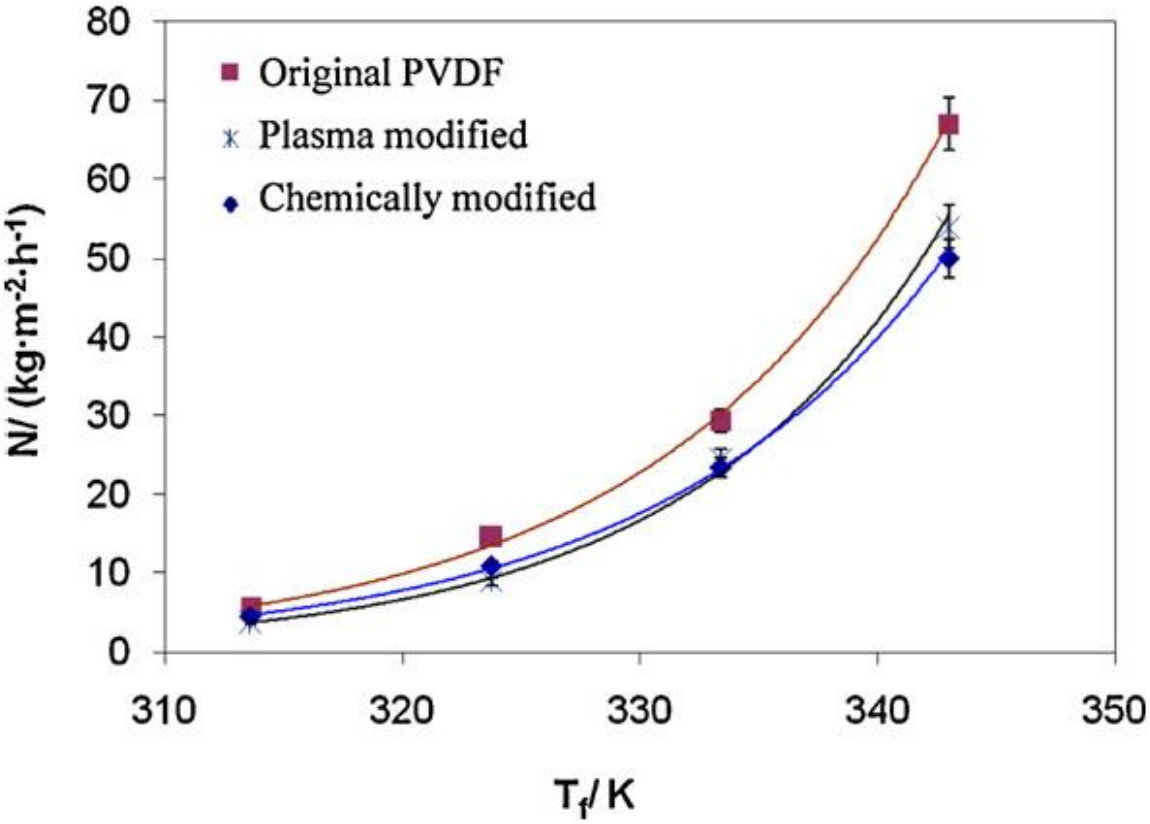
Original PVDF
Plasma modified
Chemically modified
N/ (kg·m-2·h-1)
Tf/ K
0
10
20
30
40
50
60
70
80
310
320
330
340
350

Fig. 4.

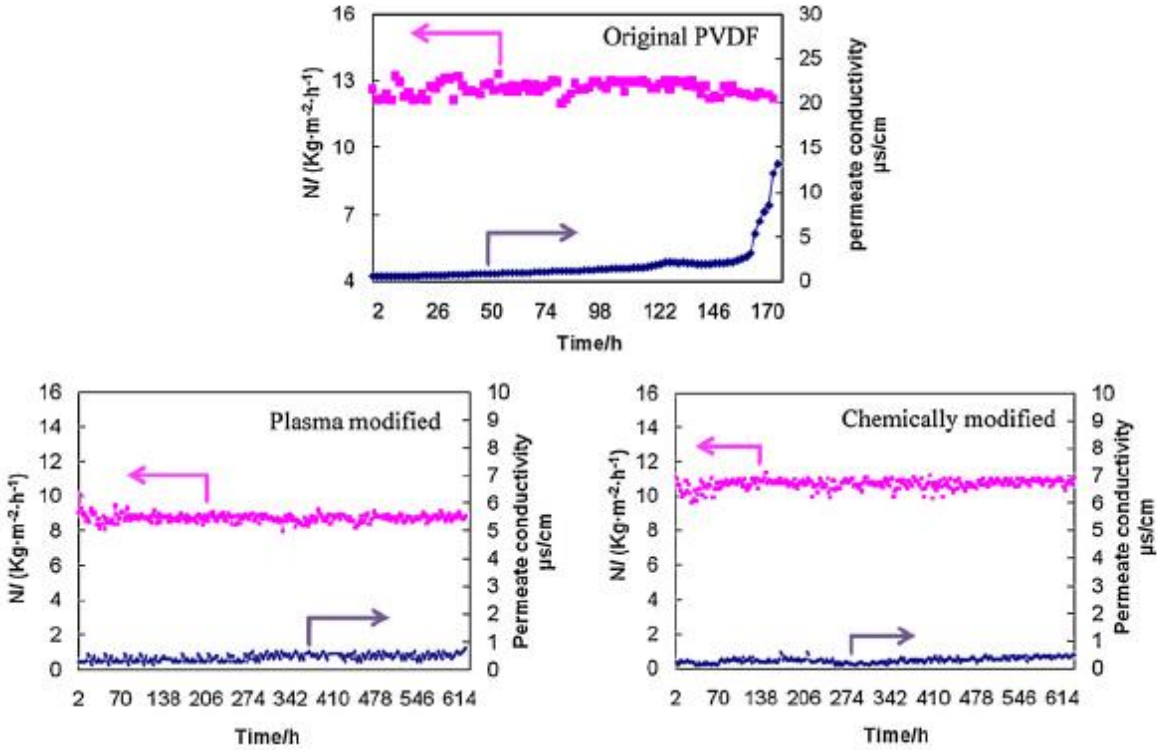
Original PVDF
Plasma modified
Chemically modified
N/ (Kg·m⁻²·h⁻¹)
permeate conductivity µs/cm
Permeate conductivity µs/cm
Time/h
2 26 50 74 98 122 146 170
2 70 138 206 274 342 410 478 546 614

Fig. 5.

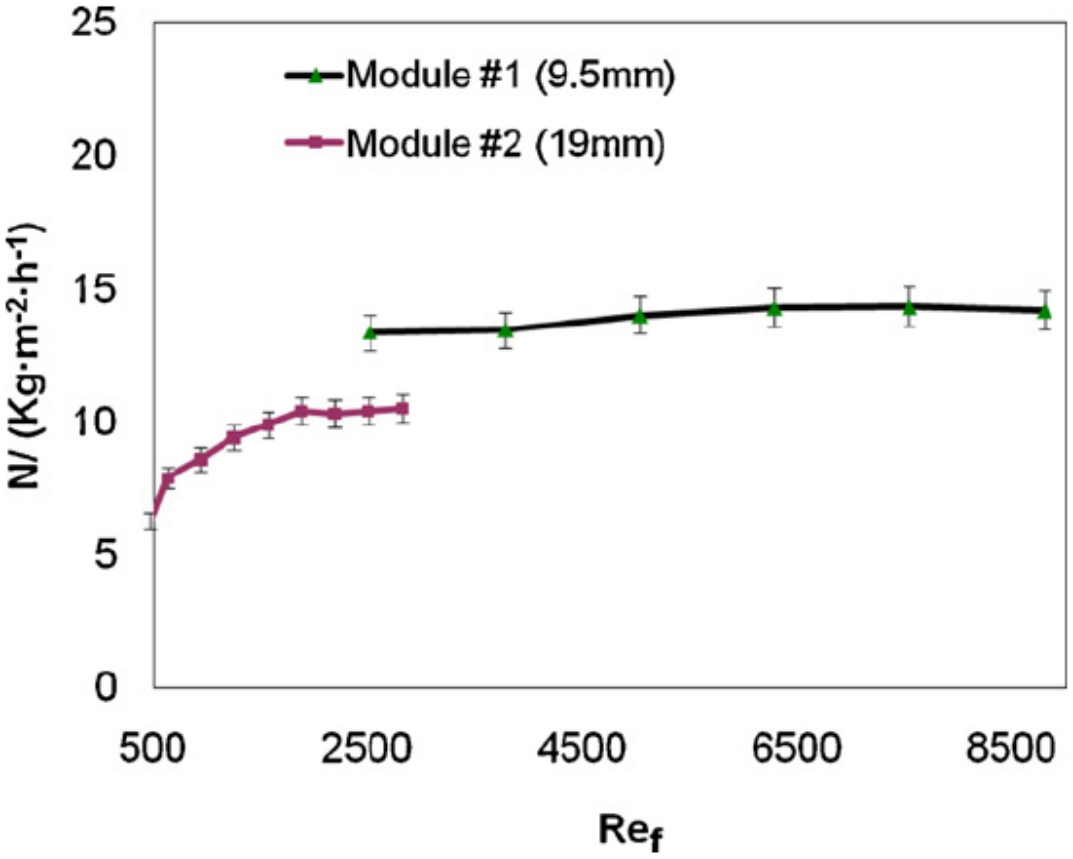
25
20
15
10
5
0
N/ (Kg·m-2·h-1)
Module #1 (9.5mm)
Module #2 (19mm)
500
2500
4500
6500
8500
Ref

Fig. 6.

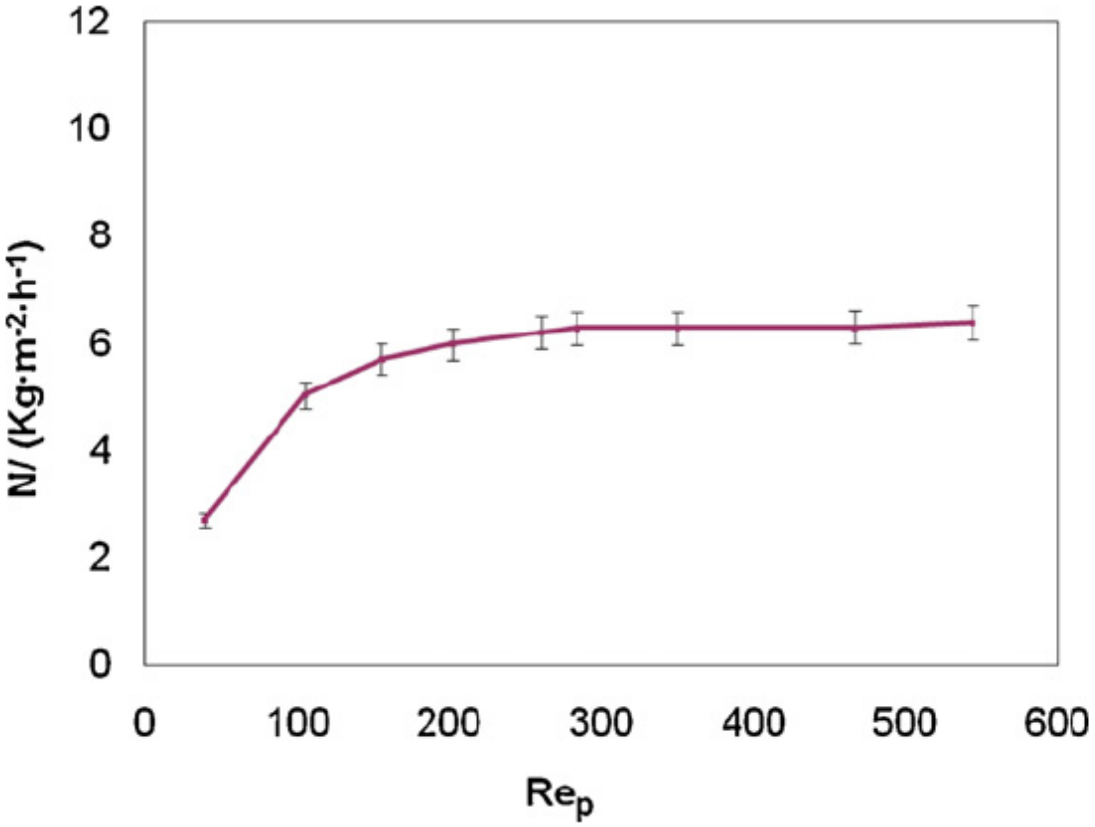

Fig. 7.

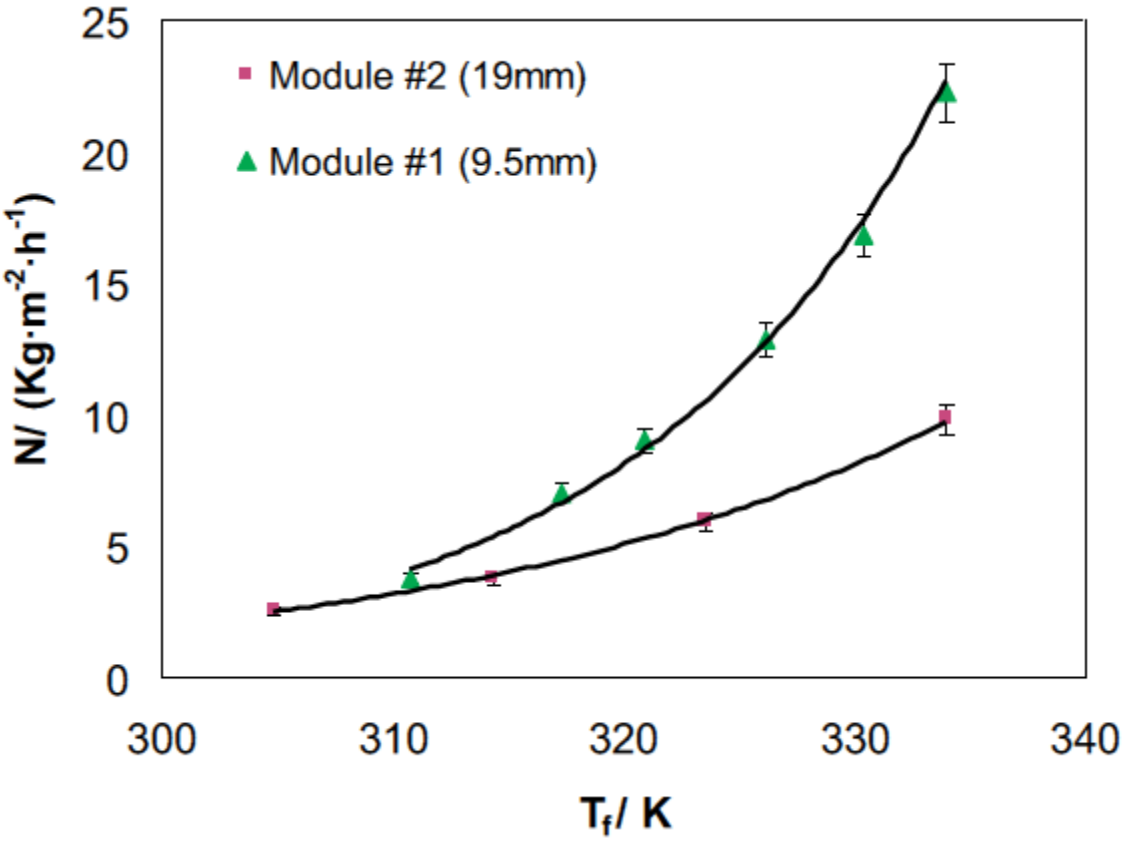
Module #2 (19mm)
Module #1 (9.5mm)
N/ (Kg·m-2·h-1)
Tf/ K
0
5
10
15
20
25
300
310
320
330
340

Fig. 8.

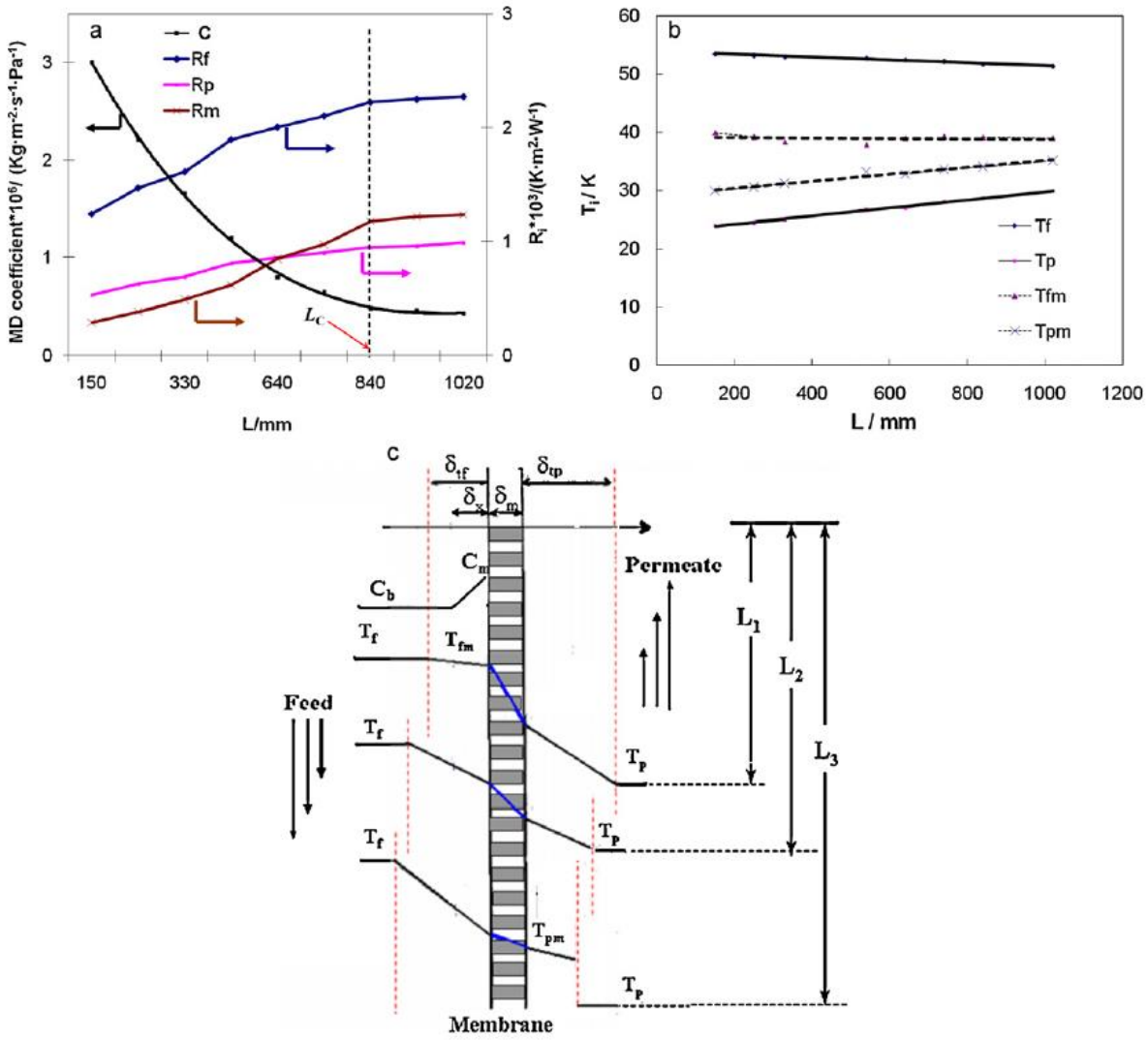
a
c
Rf
Rp
Rm
L_C
MD coefficient*10⁵/ (Kg·m⁻²·s⁻¹·Pa⁻¹)
R_i*10³/(K·m²·W⁻¹)
L/mm
b
T_i / K
Tf
Tp
Tfm
Tpm
L / mm
c
δ_{tf}
δ_{tp}
δ_g
δ_m
C_m
C_b
T_f
T_{fm}
Feed
Permeate
T_p
T_{pm}
L_1
L_2
L_3
Membrane

Fig. 9.

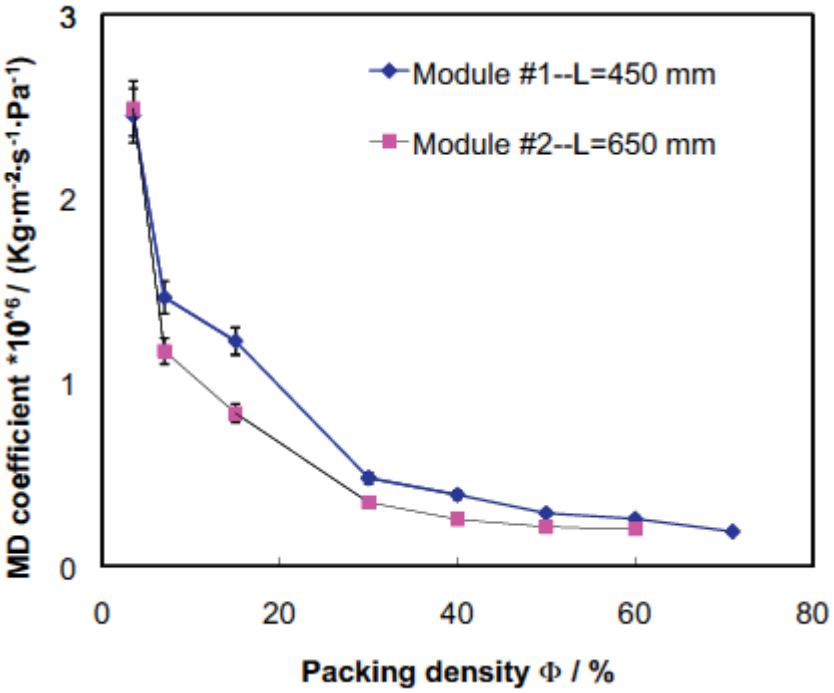
Module #1--L=450 mm
Module #2--L=650 mm
MD coefficient *10^6 / (Kg·m^-2·s^-1·Pa^-1)
Packing density Φ / %
0
1
2
3
0
20
40
60
80

Fig. 10.

Module no.	Housing diameter, d_s (mm)	Membrane type	No of fibers, n	Effective fiber length, L (mm)	Packing density, Φ (%)	Membrane area, A (m^2)	Remark
#1	9.5	Original /modified	20	225	50	0.022	Flux tests, circulating velocity and module size comparison
#2	19	Original	80	360	50	0.135	Module size comparison
#3	9.5	Original	1	150–1020	–	–	Single fiber tests
#4	19	Original	–	450/650	3.5–71	–	Packing density tests

Table 1

Membrane type	Dimension	Contact angle (°)	Porosity £ (%)	LEPw (Bar)	Tensile modulus, E_t, (MPa)	Strain at break (%)
Original PVDF	OD: 1.47 mm δ: 275 μm	88	85	1.38	44.60	98.60
Plasma modified	OD: 1.47 mm δ: 275 μm	105	83	3.86	41.05	102.08
Chemically modified	OD: 1.47 mm δ: 275 μm	115	80	3.64	45.06	121.94

Table 2